Chemical Engineering Journal 382 (2020) 122999

Contents lists available at ScienceDirect

Chemical Engineering Journal

journal homepage: www.elsevier.com/locate/cej

Chitosan functionalized iron nanosheet for enhanced removal of As(III) and Sb(III): Synergistic effect and mechanism

Jianqiang Zeng[a], Pengfei Qi[a,*], Junjie Shi[b], Thomas Pichler[c], Fuwei Wang[a], Yan Wang[d], Kunyan Sui[a,*]

[a] State Key Laboratory of Bio-Fiber and Eco-textiles, College of Materials Science and Engineering, Collaborative Innovation Center for Marine Biobased Fibers and Ecological Textiles, Institute of Marine Biobased Materials, Qingdao University, No. 308 Ningxia Road, Qingdao 266071, PR China
[b] Shandong Applied Research Center of Gold Nanotechnology (Au-SDARC), College of Chemistry & Chemical Engineering, Yantai University, Yantai 264005, PR China
[c] Geochemistry and Hydrogeology, Department of Geosciences, University of Bremen, Klagenfurter Straße 2-4, 28359 Bremen, Germany
[d] College of Chemistry and Chemical Engineering, Qingdao University, Qingdao 266071, PR China

HIGHLIGHTS

- CS functionalized iron nanosheet was fabricated for efficient As(III) and Sb (III) removal.
- Good dispersion and high adsorption capacity were observed in the presence of 0.5 wt% CS.
- The removal mechanism was mainly dominated by a synergy effect of surface complexation and hydrogen bonding.

GRAPHICAL ABSTRACT

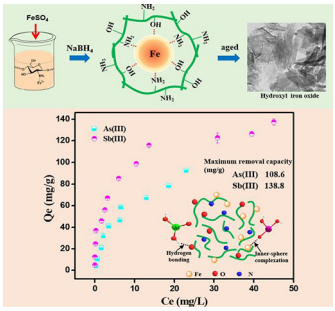

ARTICLE INFO

Keywords:
As(III) and Sb(III)
Iron/chitosan nanosheet
Synergistic effect
Adsorption mechanisms

ABSTRACT

Neutral trivalent arsenic (As(III)) and antimony (Sb(III)) species are more toxic and harder to remove from wastewater environment than their pentavalent counterparts. Herein, a natural polysaccharide chitosan (CS) functionalized iron nanosheet using an in-situ doping method was designed, aiming to attract As(III) and Sb(III) from aqueous solution. The surface area of the optimum sample was 111.8 cm^2/g, a good dispersion of the iron nanocomposite was observed by the TEM and element mapping characterization. In the batch adsorption experiment the factors of doping contents of CS and solution properties (pH, co-existing anions and humic acid) were studied systematically. The result showed that 0.5 wt% CS functionalized iron nanosheet had higher removal capacity, affinity, selectivity and reusability for Sb(III) than As(III). The optimum adsorption were achieved at the adsorbent dosage of 0.4 g/L at a wide pH values, and the maximum adsorption capacity were 108.6 and 138.8 mg/g for As(III) and Sb(III) calculated from Langmuir non-linear fitting, respectively. Both As (III) and Sb(III) removal were independent on pH values, indicating electrostatic attraction was not the dominate removal mechanism. The detailed removal mechanism was confirmed by a synergetic interaction of As-Fe/Sb-Fe complexes and hydrogen bonding using the combined characterization of FTIR and XPS spectra. This study demonstrated that the CS functionalized iron nanosheet with the properties of environmental friendly, low-cost and facile preparation could have potential applications in water purification.

* Corresponding authors.
E-mail addresses: pengfei@uni-bremen.de (P. Qi), sky@qdu.edu.cn (K. Sui).

https://doi.org/10.1016/j.cej.2019.122999
Received 17 July 2019; Received in revised form 25 September 2019; Accepted 28 September 2019
Available online 30 September 2019
1385-8947/ © 2019 Elsevier B.V. All rights reserved.

1. Introduction

Environmental contamination with heavy metals has been a worldwide problem due to the natural processes and anthropological activities. Arsenic(As) and antimony(Sb) contamination have been global potential disasters in many countries [1–4]. They have a potential threat to aquatic lives and humans due to their toxicity, bioaccumulation and non-biodegradable properties [5–7]. The World Health Organization (WHO) recommended the maximum permissible limit of As and Sb in drinking water at 10.0 and 5.0 μg/L, respectively [8]. It is well known that they are mostly found as inorganic trivalent and pentavalent species in the aquatic systems. Compared with As(V) and Sb(V) oxyacid anions, As(III) and Sb(III) are harder to remove owing to the less potential for charge dependent associations with solid phases, where they mainly existed as neutral forms of $As(OH)_3$ and $Sb(OH)_3$. Additionally, As(III) and Sb(III) are more toxic and mobile. Thus, it is more required and urgent to remove As(III) and Sb(III) from wastewater.

Numerous technologies have been proposed in disposing polluted water containing toxic metals, including adsorption, coagulation/flocculation, membrane separation, ion exchange method and extraction. Among them, adsorption is the most attractive and practical method to remove toxic metals [9–12]. Various types of materials have been developed on the removal of toxic metals such as ligand exchange resins and fibers, metal-organic frameworks and metal oxides [12–19]. Iron-based materials as potential candidates have attracted a lot of interest in As and Sb remediation due to their high efficiency, environmental friendly and abundance on earth, for example, zero-valent iron, iron (hydro)oxides, bimetal oxides containing iron [20–27]. However, the pristine nano iron-based adsorbents could encounter agglomeration and thus lead to a significant decrease in the reactivity and adsorption capacity, thus limit their application in eliminating As and Sb pollution. In order to overcome the problems, spherical composite have been prepared using surfactants and polymers to embed the nano iron-based materials [28–30]. Unfortunately, the surface sites of the iron particles inside the beads may not be accessible by the targeted contaminants.

Surface modification is an alternative promising strategy for stabilizing the nanomaterials and enhancing the adsorption efficiency, such as amino modification. Chitosan (CS) as an abundant cationic polyelectrolyte is environmental friendly and biodegradable containing abundant of amino and hydroxyl groups [31]. The dispersion and available specific surface sites of the nano iron could be enhanced by chelating CS with iron [32–34], moreover, the ligand CS could be synergistically attract As(III) and Sb(III) by chelating and electrostatic attractions. Thus it is reasonable to develop a CS functionalized iron nanocomposite to enhance the removal capacity of As(III) and Sb(III). And the role of CS on the reactivity of the as-prepared iron nanocomposite materials was explored as well as the synergistic removal mechanism for As(III) and Sb(III).

Here, we have developed a CS functionalized iron nanocomposite using in-situ doping method, and provided detailed experimental and theoretical study on the removal of As(III) and Sb(III). The main objectives were to (1) analyze the dispersity and synergy removal capacity for As(III) and Sb(III) after functionalization with CS; (2) comparatively investigate the removal performance as a function of factors, including doping contents of CS, pH, co-existing anions and humic acid, as well as the cycle removal performance; and (3) access the contribution of electrostatic attraction, surface coordination, hydrogen bonding on the overall removal mechanism of As(III) and Sb(III).

2. Experimental section

2.1. Chemicals and reagents

All chemicals were analytical grade and used without further purification. The 1000 mg/L stock solutions of As(III) and Sb(III) were prepared by dissolving sodium arsenite ($NaAsO_2$) and potassium antimonyl tartrate trihydrate ($C_8H_4K_2O_{12}Sb_2{\cdot}3H_2O$) in deionized distilled (DDI) water, respectively. All working solutions were freshly prepared each time.

2.2. Synthesis of CS functionalized iron nanocomposite

Fabrication of the nanocomposite was carried out by stabilizing the in-situ growth of iron particles in the presence of CS as a stabilizer. Different molecular weights of CS were initially used, however, a large part of precipitates were dissolved by the excess acetic acid when a small molecular weight of CS was used as a ligand (data now shown). Hence subsequently experiments were conducted using a large molecular weight of CS. Firstly, a CS solution was prepared by adding acetic acid slowly until the CS was just dissolved. Then nitrogen was injected into the CS solution to remove any dissolved oxygen before a $FeSO_4$ solution was added under stirring. This was followed by the addition of $NaBH_4$ leading to the formation of black precipitation. The homogeneous solution was stirred for 60 min. The products were washed several times with de-ionized water and dried at 50 °C. The prepared powder was ground and stored in a brown bottle.

2.3. Batch experiments

Batch experiments were performed in 50 mL sealed vials to evaluate the removal performance of As(III) and Sb(III) by the iron nanocomposite. The adsorption isotherms for As(III) and Sb(III) were performed at room temperature, with an initial concentration range from 2 to 60 mg/L and from 2 to 100 mg/L respectively. The adsorption kinetics experiments were conducted with an initial concentration of 40 mg/L under neutral pH conditions and supernatant samples were obtained at different time intervals.

The effect of solution chemistry was also studied, including pHs, co-existing anions, humic acid and ionic strength. Typically, the pH values of suspension were adjusted using 0.1–1.0 M HCl or NaOH solutions. Different concentrations of co-existing anions, including CO_3^{2-}, SO_4^{2-}, SiO_3^{2-}, PO_4^{3-}, were mixed with 40 mg/L As(III) and Sb(III) solution, respectively. Humic acid concentrations ranging from 5 to 40 mg/L were mixed with 40 mg/L As(III) and Sb(III) aqueous solutions, respectively. The effect of ionic strength on the removal capacity was studied using different concentrations of NaCl. All the experiments were conducted in triplicates. After shaking for 24 h, the suspensions were filtered using 0.45 μm syringe filters. The total concentration of As(III) and Sb(V) were determined using inductively coupled plasma-optical emission spectrometry (ICP-OES, Avio 200).

2.4. Characterization

The surface morphology of the functionalized iron nanocomposite was analyzed using scanning electron microscope (SEM) together with elemental mapping. The specific surface areas were examined by the Brunauer-Emmett-Teller (BET) N_2 adsorption/desorption method, and the pore size distribution was determined by the Brunauer-Joyner-Hallenda (BJH) method using desorption data. The zeta potential of samples in distilled water at different pH values was determined by a zetasizer at ambient temperature. The structures and interactions of the samples before and after adsorption were monitored using a Fourier transform infrared spectrometer (FTIR) and an X-ray photoelectron spectroscope (XPS).

3. Results and discussion

3.1. Characterization of the iron nanocomposite

TEM characterization showed that the CS functionalized iron nanosheet had a short rod shape (Fig. 1a), having a distinct morphology

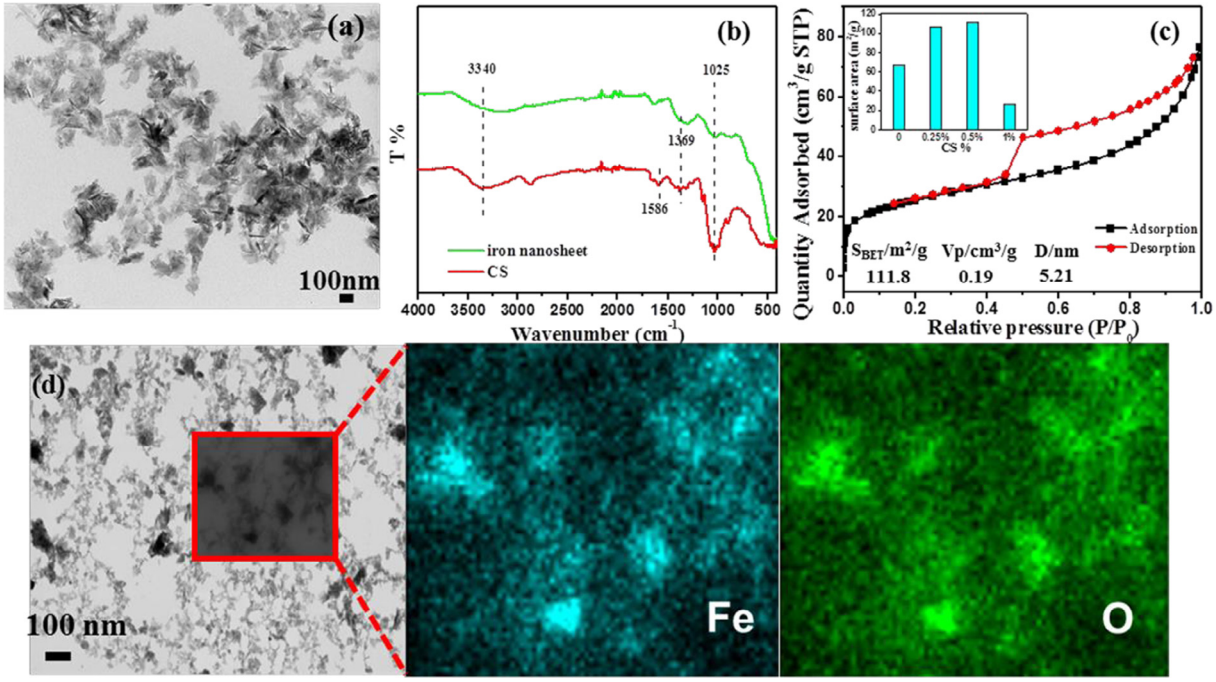

Fig. 1. TEM images (a), FTIR spectrum (b), N_2 adsorption/desorption isotherms with surface area and pore size information (c) and the corresponding element mapping images of Fe and O in the rectangular region (d) for the as-prepared iron nanocomposite with 0.5 wt% CS. And the inset in figure c shows the surface areas of samples as a function of CS content.

comparing to the pure nanoscale iron particles. The microstructure of the as-prepared nanosheet was analyzed by FT-IR spectrum (Fig. 1b). Substantial reduction of the intensity for the bands of NH_2 stretching at 3340 and 1586 cm^{-1} after modification was observed [35]. And the adsorption band –OH shifted from 1065 to 1019 cm^{-1}. Two characteristic absorption bands at 1637 and 1312 cm^{-1} were observed in the iron nanosheet, which corresponds to –CO and –CN stretching vibration [36]. These results suggest the successful binding of CS and iron via complexation involving amine and hydroxyl groups. The effect of CS content on the surface areas was shown in the inset of Fig. 1c, where the functionalized iron nanosheet with 0.5 wt% CS had a maximum surface area of 111.8 cm^2/g. And the elemental mapping analysis also present that Fe and O were uniformly dispersed in the iron nanosheet (Fig. 1d). The synergistic effects of coordination and electrostatic repulsion as well as space steric hindrance may contribute to the excellent dispersion of the iron nanosheet. However, with the further increase of CS content, a reduction of the surface area was observed, suggesting that the CS content was significant for restricting the aggregation of the as-prepared nanosheet. The nitrogen adsorption–desorption isotherm with the pore size information for the optimal sample was performed (Fig. 1c). The results showed that the average pore diameter was about 5.2 nm, and the total volume was 0.19 cm^3/g, suggesting that the as-prepared iron nanosheet was mesoporous material [37–39].

3.2. Effect of ligand CS

In order to evaluate the role of CS on the removal performance of As (III) and Sb(III), the effect of CS content on the uptake capacity were studied. As shown in Fig. 2a, the removal capacity of As(III) increased with increasing CS concentration from 0% to 0.5 wt%, followed by a decreasing trend further increasing the CS content. The similar trend was also observed for Sb(III) adsorption. These results demonstrated that the proper addition of CS had a promotion effect on As(III) and Sb (III) removal. Additionally, the presence of CS could provide additional binding sites to enhance the removal capacity of As(III) and Sb(III) via Van der Walls forces and complexation, where As(III) and Sb(III) would bind to the amine groups and hydroxyl groups of CS [40,41]. The effect of CS/Fe mass ratio on the removal capacity was also studied with a constant of 0.5% CS as shown in Fig. 2b. Apparently, the iron nanosheet show a maximum removal efficiency at a CS/Fe mass ratio of 1. It further suggests that the amount of CS is important for optimization of the dispersion and removal capacity for As(III) and Sb(III).

3.3. Removal kinetics of As(III) and Sb(III)

In order to obtain the adsorption rate and to understand the possible removal mechanism, the removal kinetics of As(III) and Sb(III) by the iron nanocomposite were investigated, and two common kinetics models were applied to analyze the kinetic data, including pseudo-first order and pseudo-second order models. As shown in Fig. 3a and b, all the kinetic curves were fitted well to the pseudo-second-order model via non-linear fitting, suggesting that the adsorption rata of As(III) and Sb(III) are mainly controlled by chemisorption and the number of the active sites determined the removal capacity [42]. The obtained kinetics parameters are shown in Table S2. Notably, the adsorption rate (k_b) of Sb(III) was higher relative to that of As(III), implying that the chemisorption between Sb(III) and the iron nanocomposite is more robust [43].

3.4. Adsorption isotherms

To access the uptake capacity of As(III) and Sb(III) by the functionalized iron nanosheet, adsorption isotherms were studied at room temperature. Non-linear fitting of typical Langmuir and Freundlich models were conducted to explore the adsorption isotherm data (Fig. 3c and d). The comparison of adsorption constants calculated based on the two models are listed in Table S2. The iron nanosheet exhibited a higher affinity of Sb(III) than As(III) based both on the maximum adsorption capacity calculated from Langmuir model and the K_f value calculated from Freundlich model [44]. The maximum adsorption of As (III) and Sb(III) were 108.6 and 138.8 mg/g according to the non-linear fitting of Langmuir model, respectively. The bonding force between Sb (III) and the surface sites should be more strongly, since Sb(III) is a stronger Lewis base than As(III) with a higher pK_a value if considering

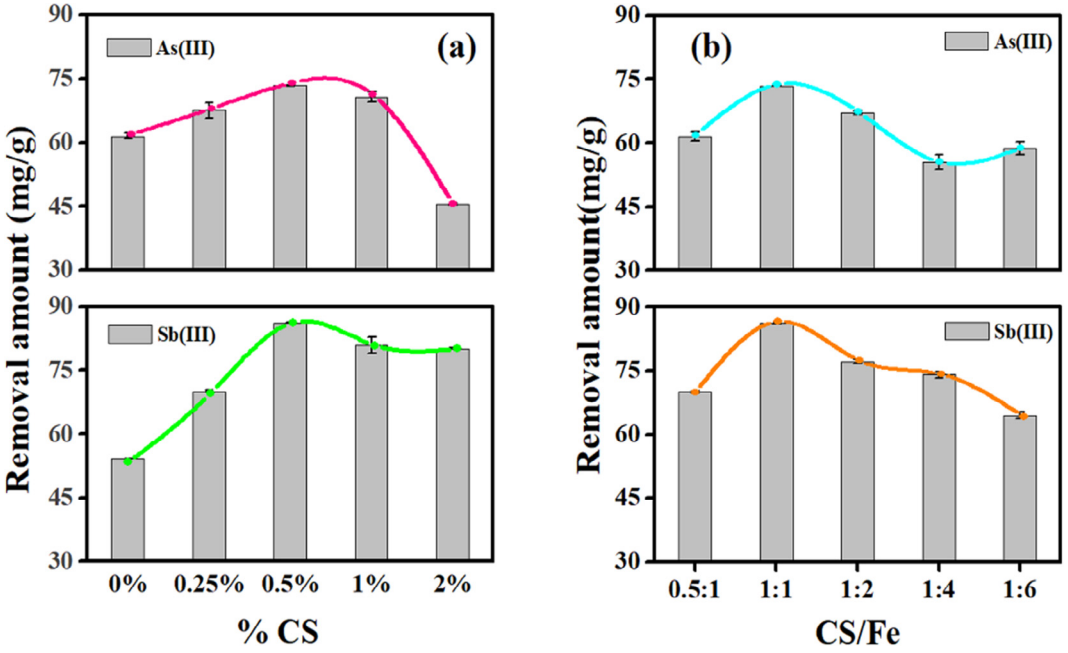

Fig. 2. (a) Effect of varying CS content; (b) effect of the CS/Fe ratio on the adsorption of As(III) and Sb(III).

the iron nanosheet as Lewis acid [45]. In addition, as shown in the insets, the removal efficiency for Sb(III) at a lower initial concentration was close to 100%, while As(III) present a lower removal efficiency around 85%. The comparison of the removal capacity for As(III) and Sb (III) mainly among the iron-based composite materials was performed (Table 1). Although some of the composite materials exhibited higher removal capacity than the CS functionalized iron nanosheet, it still showed potential applications in wastewater treatment due to the properties of low-cost, environmental friendly and simple preparation.

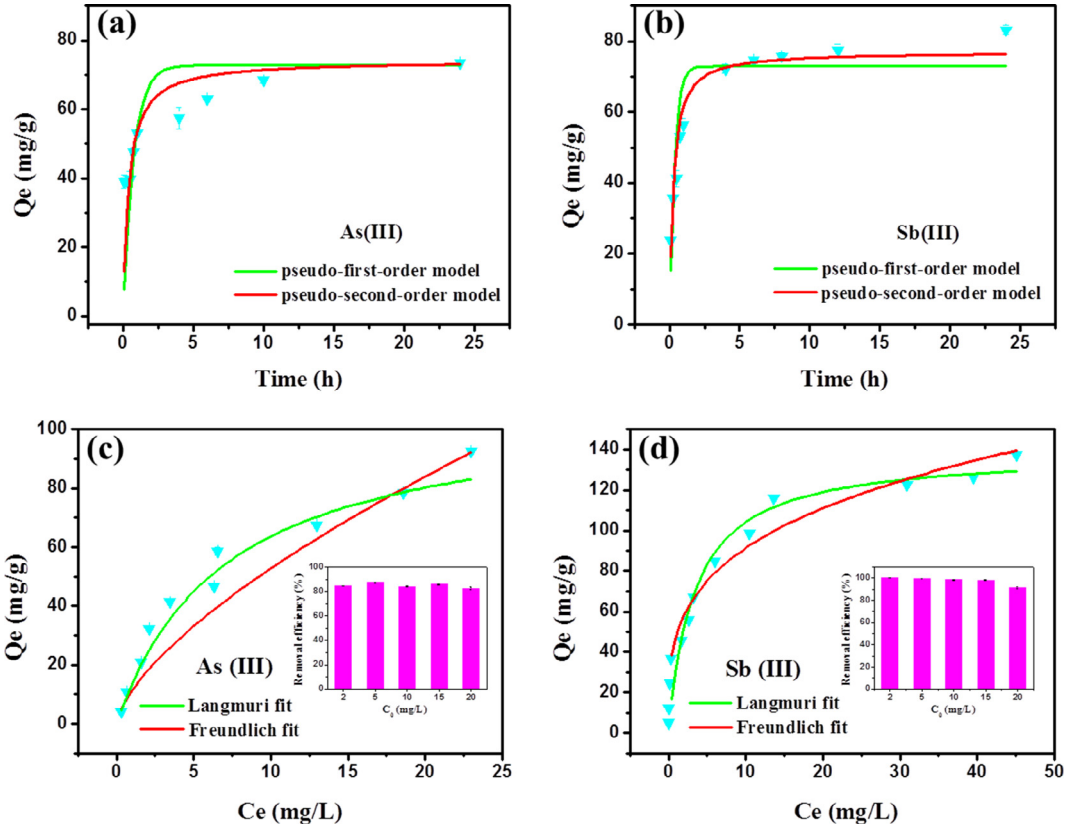

Fig. 3. Kinetic data for As(III) (a) and Sb(III) (b) removal by the iron nanocomposite (C_0 = 40 mg/L, adsorbent dosage = 0.4 g/L; pH = 7.0); adsorption isotherm of As(III) (a) and Sb(III) (b) by the iron nanocomposite with CS content of 0.5 wt%, and C_0 (As(III)) = 2–60 mg/L (a), and C_0 (Sb(III)) = 2–100 mg/L (b), adsorbent dosage = 0.4 g/L, pH = 7.0.

Table 1
Comparison of the maximum removal capacity among some of the iron-based composite materials.

Target	Materials	Removal capacity (mg/g)	Reusability	Ref.
As(III)	Fe_3O_4/HNTs	408.7	6 times 83%	[46]
	Iron chitosan flakes	16.2	2 times stable	[47]
	Iron nanoparticles	24.2	–	[48]
	Potassium ferrate	108.3	–	[49]
	Cs functionalized iron nanosheet	108.6	4 times 50.3%	Present study
Sb(III)	Iron-coated cork granulates	5.8	–	[50]
	$MnFe_2O_4$-BC	237.5	5 times 60%	[51]
	MNP@hematite	36.7	6 times stable	[52]
	Potassium ferrate	55.4	–	[49]
	Cs functionalized iron nanosheet	138.8	4 times 85.6%	Present study

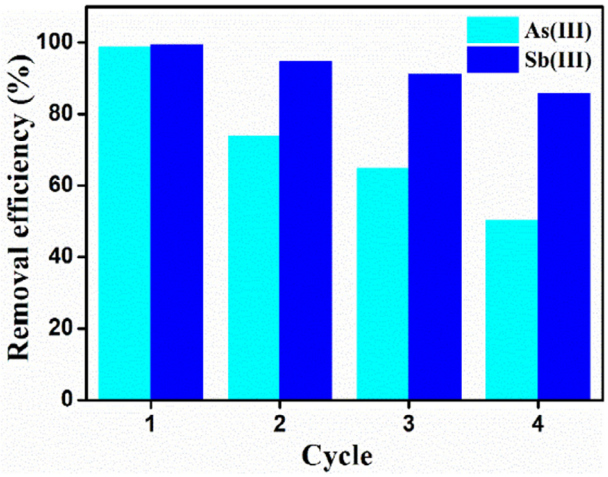

Fig. 5. Regeneration of the iron nanosheet for the removal of As(III) and Sb(III) with eluent of 0.5 M NaOH.

3.5. Effect of solution chemistry

Humic acid (HA) is the considered most representative organic matter in natural water and thus the effect of HA on the removal of As (III) and Sb(III) was evaluated at different HA concentrations. As can be seen in Fig. 4b, it has a negligible effect on the removal process of of Sb (III) at a concentration range from 5 to 40 mg/L, which is consistent with previous studies [53,54]. The addition of HA also had a minor effect on As(III) removal at the concentration range from 5 to 20 mg/L, while it was reduced by 8% when the concentration of HA raised to 40 mg/L. Possibly the negatively charged macromolecules of HA can bind the positively charged surface sites of the iron nanocomposite as well as occupy and compete with As(III) for partial of adsorption sites [55].

The adsorption capacity of Sb(III) and As(III) were further studied to evaluate the specific selectivity in the existing of common anions of SO_4^{2-}, CO_3^{2-}, SiO_3^{2-} and PO_4^{3-}. As shown in Fig. 4c, the existing foreign ions were not observed to have a distinct influence on the removal of Sb(III), suggesting the specific chemical reaction between Sb (III) and the iron composite [27]. The adsorption of As(III) was somewhat impeded by the existing ions of SiO_3^{2-} and PO_4^{3-} at a concentration of 50 mg/L, and SO_4^{2-} and CO_3^{2-} did not cause any obvious interference on As(III) removal (Fig. 4d). The negative influence of PO_4^{3-} on both As(III) and As(V) removal have been known due to their chemical similarity [55–58]. The SiO_3^{2-} ion could compete with As(III) since it was easy to accumulate in hydrous ferric oxides [59].

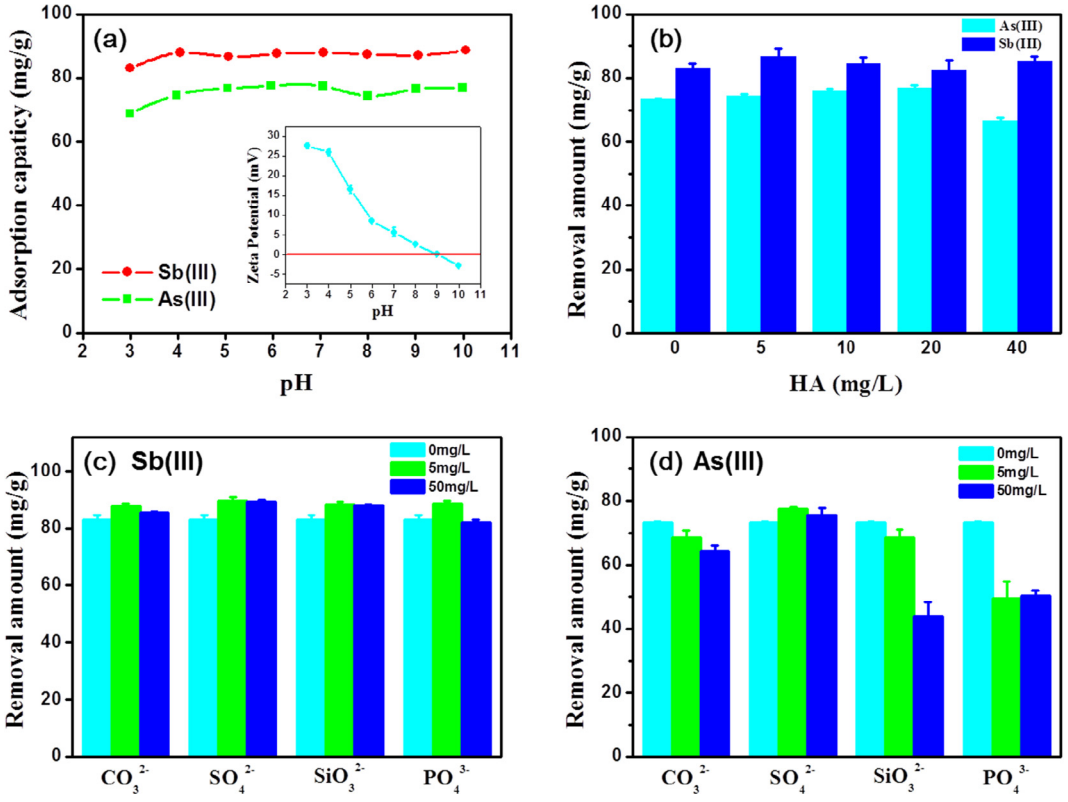

Fig. 4. (a) As(III) and Sb(III) removal by the iron nanocomposite as a function of pH values and the inset in a is the zeta potential. Effect of HA (b) and anions (c and d) on the removal of As(III) and Sb(III), including CO_3^{2-}, SO_4^{2-}, SiO_3^{2-} and PO_4^{3-} (initial concentration of As(III) and Sb(III): 40 mg/L; adsorbent dosage: 0.4 g/L; pH: 7).

Consequently, the CS functionalized iron nanocomposite exhibited higher selectivity for Sb(III) than As(III) due to the strong binding force between Sb(III) and the surface sites.

3.6. Reusability study

Sustainability is a definite must to elucidate the adsorbent potentiality [44]. Hence the recycling performance for the removal of As(III) and Sb(III) were studied as shown in Fig. 5. The iron nanocomposite was regenerated after each adsorption with 0.5 M NaOH as eluent. After four cycles, the Sb(III) removal efficiency did not diminish significantly, while the As(III) removal efficiency almost decreased half comparing to the original value. The comparison of the reusability among the iron-based materials was presented in Table 1. The CS functionalized iron nanosheet exhibited a good reusability for Sb(III), and it further testified the stronger interaction between Sb(III) and surface sites than for As(III). Additionally, the complicated solid–liquid separation procedures could lead to the loss during the repeated application processes. Moving forwards, according to the limitations of the nanoscale nanomaterials, it is crucial to further design new directions for disposing the wastewater such as nanocomposite membrane materials.

3.7. Synergistic removal mechanism

To evaluate the control of electrostatic interaction during adsorption, the correlation between removal capacity and pH values was studied as shown in Fig. 4a. The As(III) and Sb(III) removal was almost constant over the pH range from 3 to 10. The surface of the iron nanocomposite was positively charged at a pH below 9, the value of the point of zero charge (pH_{PZC}) of the iron nanocomposite, and charged negatively above 9. The removal capacity of As(III) and Sb(III), however, did not change as a function of pH, suggesting that electrostatic attraction was not involved in the adsorption process, which in turn is corresponding to the fact that both As(III) and Sb(III) mainly exist as uncharged species (H_3AsO_3 and H_3SbO_3) in the pH range from 2 to 9. The ionic strength with increasing concentration of NaCl showed a negligible influence on the removal of As(III) and Sb(III) (Fig. S2), suggesting that both As(III) and Sb(III) could tightly bound on the surface sites via the formation of surface complexes.

The identification of involved removal mechanism of As(III) and Sb (III) by the functionalized iron nanocomposite was further studied by XPS and FTIR, respectively. The XPS regional scans of C and N further suggest the successful binding of CS and iron (Fig. 6a). After adsorption of As(III), a sole new peak at the binding energy of 44 eV appeared (Fig. 6a), indicating that As(III) was adsorbed on the surface sites without being oxidized [60]. In contrast, two typical peaks at 539 and 530 eV, corresponding to $Sb3d_{3/2}$ and $Sb3d_{5/2}$, appeared after Sb(III) adsorption, respectively. Such an increment of intensity at 530 eV after adsorption should be caused by the overlap of the O1s peak with the $Sb3d_{5/2}$ peak. Two typical peaks of Sb(III) and Sb(V) on the binding sites suggest that partial oxidation of Sb(III) is occurred during adsorption, corresponding to the previous studies that Sb(III) is more readily oxidized than As(III) at a lower Eh [61,62]. The removal performance of the trace amount of formed Sb(V) was not further discussed, because its concentration was considered too low to interfere with Sb(III) removal [63].

The interaction of As/Sb-Fe in the adsorption process was also examined. As shown in Fig. 6b, various valence states of Fe, including trivalent and bivalent as well as zero-valent iron, coexisted in the iron nanocomposite. The corresponding peaks at the binding energies of 710 eV could be ascribed to Fe(II) [64], and the observed peaks at 711, 712 and 724 eV corresponded to Fe(III). Most of the iron transferred and existed as Fe^{2+} and Fe^{3+}, suggesting that the addition of CS facilitate the nano iron to undergo surface passivation. The electro transformation could be occurred between iron and the protonated amino group of CS. And the passivation products could mainly be hydroxyl iron oxides according to the XRD characterization (Fig. S4), demonstrating a higher adsorption capacity compared to the nano iron [65]. The peak intensity of Fe2p declined after adsorption, suggesting that the formed hydroxyl ferric oxides could be contributed to the adsorption of As(III) and Sb(III) via the formation of inner-sphere complexes. This was also verified in the O1s spectra (Fig. 6c), where the peak at 529 eV ascribing to Fe-O bonds moved to a higher binding energy after adsorption. The peaks located at 718 eV could be attributed to Fe^0 [66], and the lower intensity after adsorption suggests that Fe^0 was also involved in the adsorption process.

The synergistic effect on the enhanced removal capacity of As(III) and Sb(III) via hydrogen bonding was also considered. Look at the C 1s XPS spectra (Fig. 6d), a difference trend was observed for the band of C-OH after adsorption, which was consistent with the O 1s spectra that the peak shifted to the aspect of lower binding energy resulting from electron migration (Fig. 6c). This observation also corresponded to the results obtained from FTIR spectra, where the band of –OH shifted and the density was weakened after the adsorption of Sb(III). Thus it was concluded that the surface hydroxyl groups of CS could have a beneficial effect on the adsorption of As(III) and Sb(III) by forming hydrogen bonds.

In summary, a synergistic mechanism for the high affinity of the neutral H_3AsO_3 and H_3SbO_3 species on the CS functionalized iron nanosheet is illustrated in Fig. 7. Abundant surface groups and active sites were available as well as surface passivation were facilitated after modification by CS. Surface complexation between hydroxyl iron oxides and As(III)/Sb(III) play an important role during the adsorption. Hydrogen bonds between surface hydroxyl groups on the iron nanocomposite and As(III)/Sb(III) molecules also contributed to the adsorption of As(III) and Sb(III). Overall, the CS functionalized iron nanocomposite show potential applications in water purification with the properties of simple fabrication, high efficiency, environment friendly and low-cost.

4. Conclusions

In this study, a CS functionalized iron nanocomposite material was successfully fabricated for effective removal of As(III) and Sb(III). The addition of CS on the enhanced adsorption capacity mainly include two aspects: On one hand, the iron nanocomposite had a highest surface area and good dispersion with a CS content of 0.5 wt%. On the other hand, abundant surface functional groups were available and the hydroxyl iron oxides during surface passivation was formed. The kinetics of As(III) and Sb(III) were fitted well by the pseudo-second order equation, suggesting the adsorption rate was controlled by chemisorption. The iron nanosheet exhibited a higher affinity for Sb(III) than As (III) based on the non-fitting of Langmuir and Freundlich models. Moreover, the adsorption of Sb(III) was not interfered by the existing foreign ions, and the As(III) adsorption was somewhat disturbed by the presence of PO_4^{3-} and SiO_3^{2-}. The iron nanosheet also showed a better reusability for Sb(III) than As(III) during regeneration processes. The enhanced removal of As(III) and Sb(III) by the CS functionalized iron nanosheet was ascribed to the synergistic effect of As-Sb/Fe complexation and hydrogen bonding. Overall, the facile fabrication of iron nanocomposite exhibited promising applications as a potential adsorbent in wastewater treatment.

Declaration of Competing Interest

The authors declare that they have no known competing financial interests or personal relationships that could have appeared to influence the work reported in this paper.

Acknowledgements

This research was supported by Natural Science Foundation of

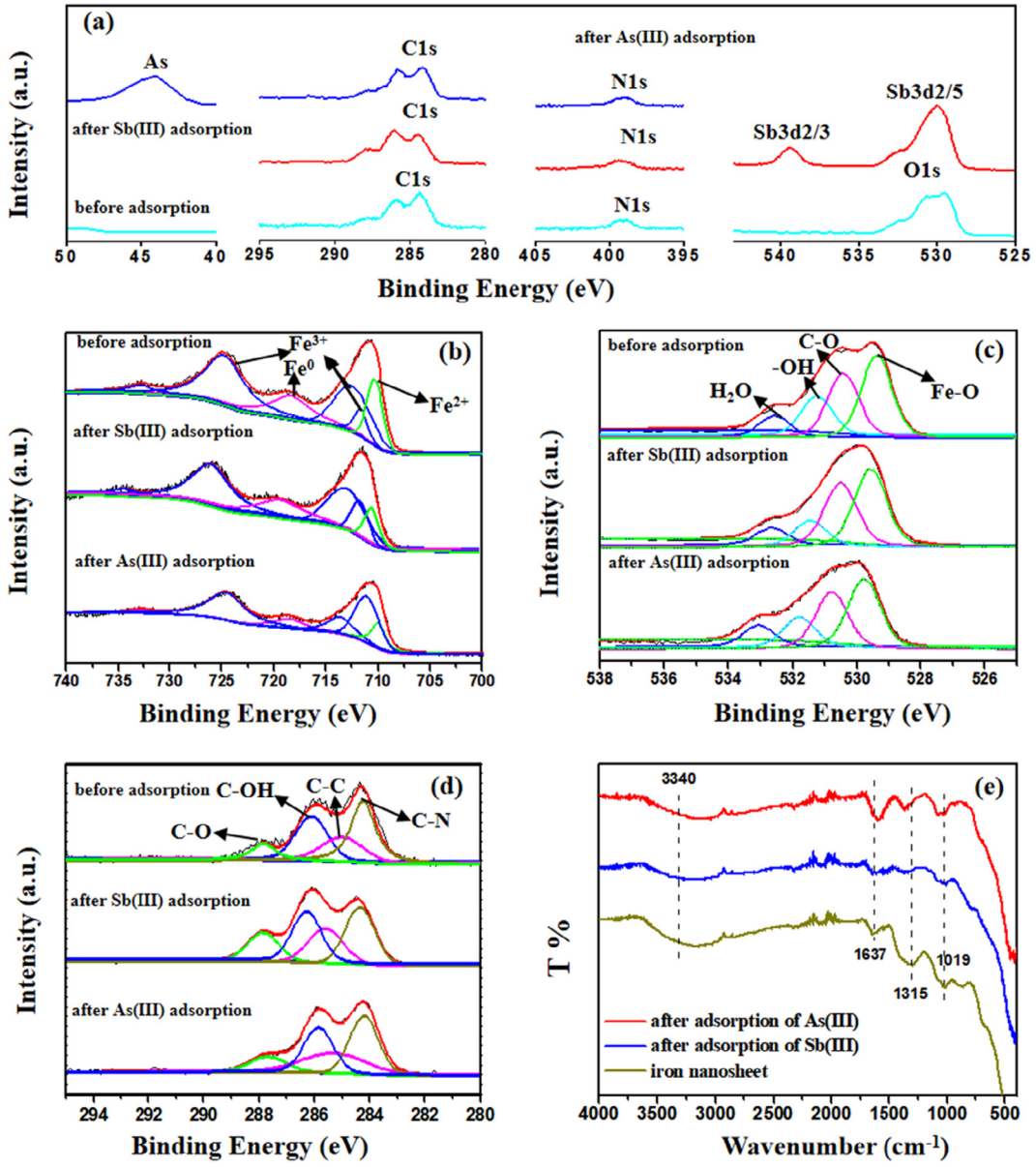

Fig. 6. XPS regional sans of the CS functionalized iron nanocomposite and after adsorption of As(III) and Sb(III) (a); XPS response of O1s (b), Fe2p (c) and C 1 s (d) before and after adsorption of As(III) and Sb(III); (e) Infrared spectrum as-prepared iron nanosheet and after adsorption of As(III) and Sb(III).

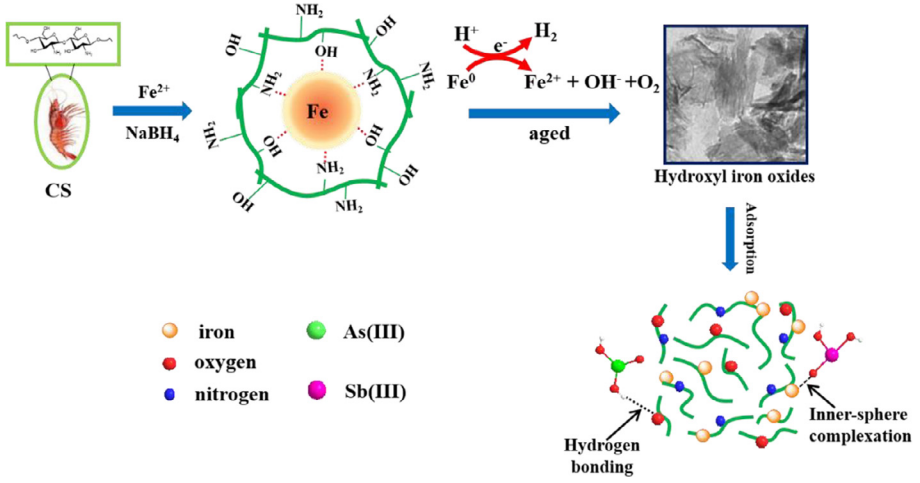

Fig. 7. Synergistic removal mechanism towards As(III) and Sb(III) based on the CS functionalized iron nanosheet.

Shandong Province (ZR2019QD019), and Program for Taishan Scholar of Shandong Province.

Appendix A. Supplementary data

Supplementary data to this article can be found online at https://doi.org/10.1016/j.cej.2019.122999.

References

[1] E. Hiller, B. Lalinská, M. Chovan, Ľ. Jurkovič, T. Klimko, M. Jankulár, R. Hovorič, P. Šottník, R. Fľaková, Z. Ženišová, Arsenic and antimony contamination of waters, stream sediments and soils in the vicinity of abandoned antimony mines in the Western Carpathians, Slovakia, Appl. Geochem. 27 (2012) 598–614.

[2] M. He, X. Wang, F. Wu, Z. Fu, Antimony pollution in China, Sci. Total Environ. 421 (2012) 41–50.

[3] S. Bindal, C.K. Singh, Predicting groundwater arsenic contamination: regions at risk in highest populated state of India, Water Res. 159 (2019) 65–76.

[4] K. Macgregor, G. MacKinnon, J.G. Farmer, M.C. Graham, Mobility of antimony, arsenic and lead at a former antimony mine, Glendinning, Scotland, Sci. Total Environ. 529 (2015) 213–222.

[5] U.A. Khan, K. Kujala, S.P. Nieminen, M.L. Räisänen, A.K. Ronkanen, Arsenic, antimony, and nickel leaching from northern peatlands treating mining infulunced water in cold climate, Sci. Total Environ. 657 (2019) 1161–1172.

[6] D. Guo, Z. Fan, S. Lu, Y. Ma, X. Nie, F. Tong, X. Peng, Changes in rhizosphere bacterial communities during remediation of heavy metal-accumulating plants around the Xikuangshan mine in southern China, Sci. Rep. 9 (2019) 1–11.

[7] J. Li, B. Zheng, Y. He, Y. Zhou, X. Chen, S. Ruan, Y. Yang, C. Dai, L. Tang, Antimony contamination, consequences and removal techniques: a review, Ecotoxicol. Environ. Saf. 156 (2018) 125–134.

[8] S. Yamamura, J. Bartram, M. Csanady, H.G. Gorchev, A. Redekopp, Drinking Water Guidelines and Standards, World Health Organization, Geneva, Switzerland, 2003.

[9] K. Abbas, H. Znad, M.R. Awual, A ligand anchored conjugate adsorbent for effective mercury(II) detection and removal from aqueous media, Chem. Eng. J. 334 (2018) 432–443.

[10] M.R. Awual, Assessing of lead(III) capturing from contaminated wastewater using ligand doped conjugate adsorbent, Chem. Eng. J. 289 (2016) 65–73.

[11] A. Shahat, M.R. Awual, M. Naushad, Functional ligand anchored nanomaterial based facial adsorbent for cobalt(II) detection and removal from water samples, Chem. Eng. J. 271 (2015) 155–163.

[12] M.R. Awual, M. Shenashen, T. Yaita, H. Shiwaku, A. Jyo, Efficient arsenic(V) removal from water by ligand exchange fibrous adsorbent, Water Res. 46 (2012) 5541–5550.

[13] M.R. Awual, S.A. El-Safty, A. Jyo, Removal of trace arsenic(V) and phosphate from water by a highly selective ligand exchange adsorbent, J. Environ. Sci. 23 (2011) 1947–1954.

[14] A. Shahat, H.M. Hassan, H.M. Azzazy, M. Hosni, M.R. Awual, Novel nano-conjugate materials for effective arsenic(V) and phosphate capturing in aqueous media, Chem. Eng. J. 331 (2018) 54–63.

[15] M.R. Awual, M.A. Hossain, M. Shenashen, T. Yaita, S. Suzuki, A. Jyo, Evaluating of arsenic(V) removal from water by weak-base anion exchange adsorbents, Environ. Sci. Pollut. R 20 (2013) 421–430.

[16] M.R. Awual, S. Urata, A. Jyo, M. Tamada, A. Katakai, Arsenate removal from water by a weak-base anion exchange fibrous adsorbent, Water Res. 42 (2008) 689–696.

[17] T.P. Joshi, G. Zhang, W.A. Jefferson, A.V. Perfilev, R. Liu, H. Liu, J. Qu, Adsorption of aromatic organoarsenic compounds by ferric and manganese binary oxide and description of the associated mechanism, Chem. Eng. J. 309 (2017) 577–587.

[18] X. Dou, D. Mohan, X. Zhao, C.U. Pittman Jr, Antimonate removal from water using hierarchical macro-/mesoporous amorphous alumina, Chem. Eng. J. 264 (2015) 617–624.

[19] K. Taleb, J. Markovski, M. Milosavljević, M. Marinović-Cincović, J. Rusmirović, M. Ristić, A. Marinković, Efficient arsenic removal by cross-linked macroporous polymer impregnated with hydrous iron oxide: material performance, Chem. Eng. J. 279 (2015) 66–78.

[20] S. Li, W. Wang, F. Liang, W.X. Zhang, Heavy metal removal using nanoscale zero-valent iron (nZVI): theory and application, J. Hazard. Mater. 322 (2017) 163–171.

[21] Y. Wu, H. Pang, Y. Liu, X. Wang, S. Yu, D. Fu, J. Chen, X. Wang, Environmental remediation of heavy metal ions by novel-nanomaterials: a review, Environ. Pollut. (2018) 608–620.

[22] V.T. Luong, E.E.C. Kurz, U. Hellriegel, T.L. Luu, J. Hoinkis, J. Bundschuh, Iron-based subsurface arsenic removal technologies by aeration: a review of the current state and future prospects, Water Res. 133 (2018) 110–122.

[23] H. Pang, Z. Diao, X. Wang, Y. Ma, S. Yu, H. Zhu, Z. Chen, B. Hu, J. Chen, X. Wang, Adsorptive and reductive removal of U(VI) by dictyophora indusiate-derived biochar supported sulfide NZVI from wastewater, Chem. Eng. J. 366 (2019) 368–377.

[24] N. Karimian, S.G. Johnston, E.D. Burton, Antimony and arsenic partitioning during Fe^{2+}-induced transformation of jarosite under acidic conditions, Chemosphere 195 (2018) 515–523.

[25] T. Nur, P. Loganathan, M.B. Ahmed, M.A. Johir, T.V. Nguyen, S. Vigneswaran, Removing arsenic from water by coprecipitation with iron: effect of arsenic and iron concentrations and adsorbent incorporation, Chemosphere (2019) 431–438.

[26] S. Bolisetty, M. Peydayesh, R. Mezzenga, Sustainable technologies for water purification from heavy metals: review and analysis, Chem. Soc. Rev. 48 (2019) 463–487.

[27] L. Hao, M. Liu, N. Wang, G. Li, A critical review on arsenic removal from water using iron-based adsorbents, RSC Adv. 8 (2018) 39545–39560.

[28] W. Xue, D. Huang, G. Zeng, J. Wan, C. Zhang, R. Xu, M. Cheng, R. Deng, Nanoscale zero-valent iron coated with rhamnolipid as an effective stabilizer for immobilization of Cd and Pb in river sediments, J. Hazard. Mater. 341 (2018) 381–389.

[29] X. Lv, Y. Zhang, W. Fu, J. Cao, J. Zhang, H. Ma, G. Jiang, Zero-valent iron nanoparticles embedded into reduced graphene oxide-alginate beads for efficient chromium(VI) removal, J. Colloid Interface Sci. 506 (2017) 633–643.

[30] M.T. Sikder, Y. Mihara, M.S. Islam, T. Saito, S. Tanaka, M. Kurasaki, Preparation and characterization of chitosan–caboxymethyl-β-cyclodextrin entrapped nano-zero-valent iron composite for Cu(II) and Cr(IV) removal from wastewater, Chem. Eng. J. 236 (2014) 378–387.

[31] S. Olivera, H.B. Muralidhara, K. Venkatesh, V.K. Guna, K. Gopalakrishna, Y. Kumar, Potential applications of cellulose and chitosan nanoparticles/composites in wastewater treatment: a review, Carbohydr Polym. 153 (2016) 600–618.

[32] B. Geng, Z. Jin, T. Li, X. Qi, Preparation of chitosan-stabilized Fe^0 nanoparticles for removal of hexavalent chromium in water, Sci. Total Environ. 407 (2009) 4994–5000.

[33] J. He, F. Bardelli, A. Gehin, E. Silvester, L. Charlet, Novel chitosan goethite bionanocomposite beads for arsenic remediation, Water Res. 101 (2016) 1–9.

[34] M. Kanematsu, T.M. Young, K. Fukushi, P.G. Green, J.L. Darby, Arsenic(III, V) adsorption on a goethite-based adsorbent in the presence of major co-existing ions: modeling competitive adsorption consistent with spectroscopic and molecular evidence, Geochim. Cosmochim. Acta 106 (2013) 404–428.

[35] T. Parandhaman, N. Pentela, B. Ramalingam, D. Samanta, S.K. Das, Metal nanoparticle loaded magnetic-chitosan microsphere: water dispersible and easily separable hybrid metal nano-biomaterial for catalytic applications, ACS Sustain. Chem. Eng. 5 (2016) 489–501.

[36] J.D.M. Neto, C.R. Bellato, D.C. Silva, Iron oxide/carbon nanotubes/chitosan magnetic composite film for chromium species removal, Chemosphere 218 (2019) 391–401.

[37] M.R. Awual, T. Yaita, T. Taguchi, H. Shiwaku, S. Suzuki, Y. Okamoto, Selective cesium removal from radioactive liquid waste by crown ether immobilized new class conjugate adsorbent, J. Hazard. Mater. 278 (2014) 227–235.

[38] H. Lu, Z. Zhu, H. Zhang, J. Zhu, Y. Qiu, Simultaneous removal of arsenate and antimonate in simulated and practical water samples by adsorption onto Zn/Fe layered double hydroxide, Chem. Eng. J. 276 (2015) 365–375.

[39] M.R. Awual, N.H. Alharthi, Y. Okamoto, M.R. Karim, M.E. Halim, M.M. Hasan, M.M. Rahman, M.M. Islam, M.A. Khaleque, M.C. Sheikh, Ligand field effect for Dysprosium(III) and Lutetium(III) adsorption and EXAFS coordination with novel composite nanomaterials, Chem. Eng. J. 320 (2017) 427–435.

[40] D.W. Cho, B.H. Jeon, C.M. Chon, Y. Kim, F.W. Schwartz, E.S. Lee, H. Song, A novel chitosan/clay/magnetite composite for adsorption of Cu(II) and As(V), Chem. Eng. J. 200 (2012) 654–662.

[41] K.C.M. Kwok, L.F. Koong, T. Al Ansari, G. McKay, Adsorption/desorption of arsenite and arsenate on chitosan and nanochitosan, Environ. Sci. Pollut. R 25 (2018) 14734–14742.

[42] C. Tian, J. Zhao, X. Ou, J. Wan, Y. Cai, Z. Lin, Z. Dang, B. Xing, Enhanced adsorption of p-Arsanilic acid from water by amine-modified UiO-67 as examined using extended X-ray absorption fine structure, X-ray photoelectron spectroscopy, and density functional theory calculations, Environ. Sci. Technol. 52 (2018) 3466–3475.

[43] B. Dousova, M. Lhotka, J. Filip, D. Kolousek, Removal of arsenate and antimonate by acid-treated Fe-rich clays, J. Hazard. Mater. 357 (2018) 440–448.

[44] M.R. Awual, M.M. Hasan, A. Shahat, M. Naushad, H. Shiwaku, T. Yaita, Investigation of ligand immobilized nano-composite adsorbent for efficient cerium (III) detection and recovery, Chem. Eng. J. 265 (2015) 210–218.

[45] P. Qi, T. Pichler, Competitive adsorption of As(III), As(V), Sb(III) and Sb(V) onto ferrihydrite in multi-component systems: implications for mobility and distribution, J. Hazard. Mater. 330 (2017) 142–148.

[46] X. Song, L. Zhou, Y. Zhang, P. Chen, Z. Yang, A novel cactus-like Fe_3O_4/Halloysite nanocomposite for arsenite and arsenate removal from water, J. Cleaner Prod. 224 (2019) 573–582.

[47] A. Gupta, V.S. Chauhan, N. Sankararamakrishnan, Preparation and evaluation of iron–chitosan composites for removal of As(III) and As(V) from arsenic contaminated real life groundwater, Water Res. 43 (2009) 3862–3870.

[48] P. Sarntanayoot, S. Fuangswasdi, A. Imyim, Iron nanoparticle-modified water treatment residues for adsorption of As(III) and As(V) and their cement-based solidification/stabilization, Int. J. Environ. Sci. Technol. 16 (2019) 4285–4292.

[49] B. Lan, Y. Wang, X. Wang, X. Zhou, Y. Kang, L. Li, Aqueous arsenic(As) and antimony(Sb) removal by potassium ferrate, Chem. Eng. J. 292 (2016) 389–397.

[50] A.M. Pintor, B.R. Vieira, R.A. Boaventura, C.M. Botelho, Removal of antimony from water by iron-coated cork granulates, Sep. Purif. Technol. 233 (2020) 116020.

[51] Y.Y. Wang, H.Y. Ji, H.H. Lu, Y.X. Liu, R.Q. Yang, L.L. He, S.M. Yang, Simultaneous removal of Sb(III) and Cd(III) in water by adsorption onto a $MnFe_2O_4$–biochar nanocomposite, RSC Adv. 8 (2018) 3264–3273.

[52] C. Shan, Z. Ma, M. Tong, Efficient removal of trace antimony(III) through adsorption by hematite modified magnetic nanoparticles, J. Hazard. Mater. 268 (2014) 229–236.

[53] J.H. Xi, M.C. He, L.H. Kong, Adsorption of antimony on kaolinite as a function of time, pH, HA and competitive anions, Environ. Earth Sci. 75 (2016) 136.

[54] X. Guo, Z. Wu, M. He, Removal of antimony(V) and antimony(III) from drinking water by coagulation–flocculation–sedimentation (CFS), Water Res. 43 (2009) 4327–4335.

[55] Dawei Wang, Stanley E. Gilliland, Xinbei Yi, Kayla Logan, Denver R. Heitger,

Heather R. Lucas, W.-N. Wang, Iron mesh-based metal organic framework filter for efficient arsenic removal, Environ. Sci. Technol. 52 (2018) 4275–4284.
[56] M.R. Awual, A. Jyo, S.A. El-Safty, M. Tamada, N. Seko, A weak-base fibrous anion exchanger effective for rapid phosphate removal from water, J. Hazard. Mater. 188 (2011) 164–171.
[57] Y. Wei, H. Liu, C. Liu, S. Luo, Y. Liu, X. Yu, J. Ma, K. Yin, H. Feng, Fast and efficient removal of As(III) from water by $CuFe_2O_4$ with peroxymonosulfate: effects of oxidation and adsorption, Water Res. 150 (2019) 182–190.
[58] M.R. Awual, A. Jyo, Rapid column-mode removal of arsenate from water by crosslinked poly(allylamine) resin, Water Res. 43 (2009) 1229–1236.
[59] T. Pichler, J. Veizer, G.E. Hall, Natural input of arsenic into a coral-reef ecosystem by hydrothermal fluids and its removal by Fe(III) oxyhydroxides, Environ. Sci. Technol. 33 (1999) 1373–1378.
[60] T. Liu, Y. Yang, Z.L. Wang, Y. Sun, Remediation of arsenic(III) from aqueous solutions using improved nanoscale zero-valent iron on pumice, Chem. Eng. J. 288 (2016) 739–744.
[61] P. Qi, T. Pichler, Sequential and simultaneous adsorption of Sb(III) and Sb(V) on ferrihydrite: implications for oxidation and competition, Chemosphere 145 (2016) 55–60.
[62] T.L. Wu, W.X. Qin, M.E. Alves, G.D. Fang, Q. Sun, P.X. Cui, C. Liu, D.M. Zhou, Y.J. Wang, Mechanisms of Sb(III) oxidation mediated by low molecular weight phenolic acids, Chem. Eng. J. 356 (2019) 190–198.
[63] P. Qi, R. Luo, T. Pichler, J. Zeng, Y. Wang, Y. Fan, K. Sui, Development of a magnetic core-shell Fe_3O_4@TA@UiO-66 microsphere for removal of arsenic(III) and antimony(III) from aqueous solution, J. Hazard. Mater. 378 (2019) 120721.
[64] A. Wei, J. Ma, J. Chen, Y. Zhang, J. Song, X. Yu, Enhanced nitrate removal and high selectivity towards dinitrogen for groundwater remediation using biochar-supported nano zero-valent iron, Chem. Eng. J. 353 (2018) 595–605.
[65] S. Bae, R.N. Collins, T.D. Waite, K. Hanna, Advances in surface passivation of nanoscale zerovalent iron: a critical review, Environ. Sci. Technol. 52 (2018) 12010–12025.
[66] L. Tang, H. Feng, J. Tang, G. Zeng, Y. Deng, J. Wang, Y. Liu, Y. Zhou, Treatment of arsenic in acid wastewater and river sediment by Fe@Fe_2O_3 nanobunches: the effect of environmental conditions and reaction mechanism, Water Res. 117 (2017) 175–186.